Inorganic Chemistry

Article

pubs.acs.org/IC

Turn-on Phosphorescent Chemodosimeter for Hg^{2+} Based on a Cyclometalated Ir(III) Complex and Its Application in Time-Resolved Luminescence Assays and Live Cell Imaging

Jia-Xi Ru,[†] Li-Ping Guan,[‡] Xiao-Liang Tang,*[,†] Wei Dou,[†] Xiang Yao,[†] Wan-Min Chen,[†] Ya-Ming Liu,[†] Guo-Lin Zhang,*[,†] Wei-Sheng Liu,*[,†] Yue Meng,[‡] and Chun-Ming Wang[‡]

[†]Key Laboratory of Nonferrous Metal Chemistry and Resources Utilization of Gansu Province and State Key Laboratory of Applied Organic Chemistry, College of Chemistry and Chemical Engineering, and [‡]School of Life Sciences, Lanzhou University, Lanzhou 730000, People's Republic of China

Supporting Information

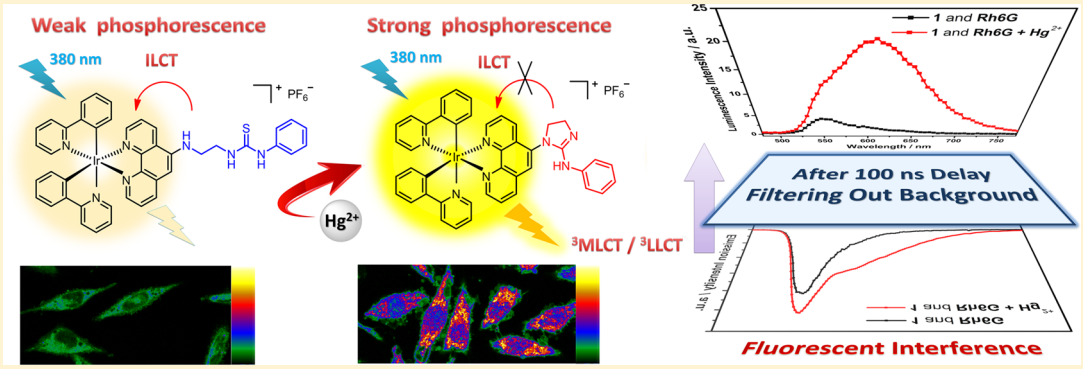

ABSTRACT: A novel "turn-on" phosphorescent chemodosimeter based on a cyclometalated Ir(III) complex has been designed and synthesized, which displays high selectivity and sensitivity toward Hg^{2+} in aqueous media with a broad pH range of 4−10. Furthermore, by time-resolved photoluminescence techniques, some interferences from the short-lived background fluorescence can be eliminated effectively and the signal-to-noise ratio of the emission detection can be improved distinctly by using the chemodosimeter. Finally, the chemodosimeter can be used to monitor Hg^{2+} effectively in living cells by confocal luminescence imaging.

INTRODUCTION

Mercury is one of the most hazardous species in nature. Due to the wide application of mercury in industry and manufacturing, the diffusion and environment contamination of mercury species in nature has aroused considerable attention, which can cause a wide variety of diseases even at very low concentration, such as neurological damage, prenatal brain damage, serious cognitive and motion disorders, and increased risk of myocardial infarction.[1] For monitoring of the dispersal of mercury species, various Hg^{2+}-sensing systems based on fluorescent signal changes have been developed.[2] However, the fluorescence signals from these probes often suffer from the interference of autofluorescence and scattered light on application in real-time environmental and biological milieus. Fortunately, time-resolved photoluminescent techniques (TRPTs) based on long-lifetime luminescent complexes, as a promising tool, can effectively eliminate the undesirable short-lived background fluorescence or scattering by introduction of an appropriate time delay from pulsed excitation to the acquisition of signals. Although luminescent lanthanide complexes have an extraordinarily long luminescence lifetime on the order of milliseconds, most of them show a natural limitation with higher excited energy, and the structural stability still needs to be improved in complex test requirements.[3] Recently, phosphorescent heavy-metal complexes with microsecond-scale luminescence lifetimes have attracted ever-increasing interest, and only a limited number of examples of TRPTs combining sensing abilities have been reported.[4] Therefore, the development of phosphorescent chemosensors for rapid and accurate detection of Hg^{2+} in complicated aqueous environments or biological milieus is an important goal.

As rapidly developing derivatives and highly sensitive optical chemosensors, cyclometalated Ir(III) sensors are considered to be excellent phosphorescent materials for bioimaging applications due to their larger Stokes shifts, long excited-state lifetimes, prominent color tunability, and suitable excitation in the visible region in comparison to most purely organic fluorophors, which may be discriminated readily from the

Received: June 16, 2014
Published: October 21, 2014

   dx.doi.org/10.1021/ic501417s | Inorg. Chem. 2014, 53, 11498−11506

scattered light and/or shorter-lived background fluorescence normally present in clinical samples and may permit the implementation of time-gated techniques.[5] As a result, a variety of cyclometalated Ir(III) complexes have been synthesized and utilized as phosphorescent chemosensors for specific anions,[6] metal cations,[7] amino acids,[8] and biomolecules.[9] To date, some Hg^{2+}-selective sensors based on cyclometalated Ir(III) complexes have been synthesized and assessed in bioimaging. For example, Hyun synthesized an aza crown ether appended Ir(III) complex which exhibits notable phosphorescence quenching for Hg^{2+} in 50% acetonitrile aqueous solution.[10] Huang, Zhao, and Li prepared a class of charge-neutral Ir(III) complexes containing a sulfur atom that shows multisignaling changes by Hg^{2+}-induced decomposition of Ir(III) complex moieties to form a new solvent complex.[11] Nabeshima synthesized a cationic Ir(III) complex based on Hg^{2+}-promoted thioacetal deprotection reaction which exhibits a ratiometric response for Hg^{2+} in acetonitrile−water (98/2 v/v).[12] Although these phosphorescent functional materials show potential application and unique superiority, many Hg^{2+}-selective sensors based on cyclometalated Ir(III) complexes act only in organic media and some only exhibit phosphorescent quenching. Moreover, their further application in time-resolved luminescence assay and biological imaging analysis is quite rare. Therefore, it is worthwhile to address these issues by proposing a novel design for developing various phosphorescent chemosensors for Hg^{2+} detection and effectively utilizing TRPT.

To get a better signal response, we attempted to develop the chemodosimeter approach by irreversible chemical reactions to give rise to sensitivity and selectivity. Herein we provide the novel phosphorescent chemodosimeter $[Ir(ppy)_2(\mathbf{L})](PF_6)$ (**1**; ppy = 2-phenylpyridine, **L** = 1-(2-(1,10-phenanthrolin-5-ylamino)ethyl)-3-phenylthiourea) (Scheme 1) as a new

Scheme 1. Synthetic Routes of Chemodosimeter 1 and Cyclized Product 2

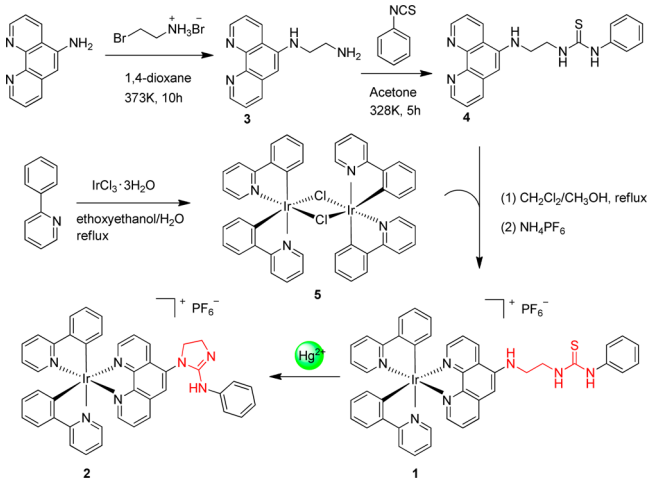

advancement in the rapid detection of Hg^{2+} ions in aqueous media. Our design is based on the well-known mercury-promoted desulfation and intramolecular cyclic guanylation of thiourea reaction exploited by Tian and Kim.[13] For chemodosimeter **1**, a thiourea unit acting as a recognition moiety was introduced into the phenanthroline ligand of the Ir(III) complexes (signaling units) to provide a specific reaction site for the Hg^{2+} ion. In the presence of Hg^{2+}, the thiourea unit of Ir(III) complexes is cyclized to form an imidazoline moiety, namely complex **2** (Scheme 1). The selectivity of phosphorescent chemodosimeter **1** for Hg^{2+} was examined in acetonitrile/HEPES buffer (10 mM, 4/6 v/v, pH 7.4) solutions, and the recognition mechanism exhibiting the phosphorescence response to Hg^{2+} ions was established through theoretical calculations and ESI mass and ^1H NMR spectra. The utility of **1** for Hg^{2+} sensing was demonstrated by the time-gated acquisition of signals that were contaminated by fluorescent Rhodamine 6G. Finally, a confocal laser scanning microscope was used to visualize intracellular Hg^{2+} ions by enhancing phosphorescence signals.

EXPERIMENTAL SECTION

Materials and Instrumentation. All reagents and solvents were obtained commercially and used without further purification unless otherwise noted. ^1H NMR and ^{13}C NMR spectra were recorded on JNM-ECS-400 MHz and Varian INOVA 600 spectrometers and referenced to the solvent signals. Mass spectra (ESI) were performed on Bruker Daltonics Esquire6000 and Bruker MicroTOF ESI-TOF mass spectrometers. All pH measurements were made with a pH-10C digital pH meter. Hg^{2+} and various other cation ions were prepared by dissolving their perchlorate salts in acetonitrile with a concentration of 10 mM.

Caution! Perchlorate salts are potentially explosive. All compounds containing perchlorates should be handled with great care and in small amounts.

Synthesis of *N*′-(1,10-Phenanthrolin-5-yl)ethane-1,2-diamine (3). 5-Amino-1,10-phenanthroline (0.96 g, 4.9 mmol) and 2-bromoethylamine hydrobromide (1 g, 4.9 mmol) were dissolved in 1,4-dioxane (30 mL) . The mixture was stirred at 373 K for 10 h under an argon atmosphere. The solvent was removed under reduced pressure, the crude product was added to water (30 mL), and the pH of the solution was adjusted to 9−10. The resulting aqueous phase was extracted with CH_2Cl_2 (100 mL × 3). Then, the solvent was removed under vacuum to yield the yellow oily crude product. The crude product was purified by silica gel chromatography with CH_2Cl_2/MeOH (1/1 v/v). The latter eluent was concentrated by evaporation and dried in vacuo, affording **3** as a yellow oily product. Yield: 0.76 g (65%). ^1H NMR (400 MHz, $CDCl_3$, δ ppm): 8.81 (dd, J = 4.3, 1.5 Hz, 1H), 8.59 (dd, J = 4.3, 1.7 Hz, 1H), 8.04 (dd, J = 8.5, 1.5 Hz, 1H), 7.63 (dd, J = 8.1, 1.6 Hz, 1H), 7.16 (ddd, J = 10.8, 8.2, 4.3 Hz, 2H), 6.22 (s, 1H), 5.12 (t, J = 5.0 Hz, 1H), 2.97 (dd, J = 11.1, 5.3 Hz, 2H), 2.82 (t, J = 5.7 Hz, 2H), 1.61 (s, 2H). ^{13}C NMR (100 MHz, $CDCl_3$, δ ppm): 149.19, 145.98, 145.52, 145.29, 140.96, 133.16, 132.79, 130.04, 128.91, 128.63, 99.34, 99.04, 45.34, 39.91. ESI mass spectrum m/z: calcd for $C_{14}H_{14}N_4$, 238.1218; found, 239.1071 $[M + H]^+$.

Synthesis of 1-(2-(1,10-Phenanthrolin-5-ylamino)ethyl)-3-phenylthiourea (4). Phenyl isothiocyanate (0.27 g, 2.0 mmol) was added dropwise to a solution of *N*′-(1,10-phenanthrolin-5-yl)ethane-1,2-diamine (0.48 g, 2.0 mmol) in 30 mL of acetone which was stirred and heated to 328 K. The reaction mixture was then stirred at that temperature for 5 h. After it was cooled, the solution was filtered and washed with ethanol, affording **4** as a pale orange solid. Yield: 0.46 g (62%). ^1H NMR (400 MHz, DMSO-d_6, δ ppm): 9.78 (s, 1H), 9.06 (dd, J = 4.2, 1.4 Hz, 1H), 8.73 (dd, J = 8.5, 1.5 Hz, 1H), 8.69 (dd, J = 4.2, 1.6 Hz, 1H), 8.08 (dd, J = 8.2, 1.6 Hz, 1H), 8.05 (s, 1H), 7.75 (dd, J = 8.4, 4.3 Hz, 1H), 7.52 (dd, J = 8.1, 4.3 Hz, 1H), 7.38 (dd, J = 8.5, 1.1 Hz, 2H), 7.35−7.27 (m, 2H), 7.16−7.07 (m, 1H), 6.89 (s, 1H), 6.69 (s, J = 4.9 Hz, 1H), 3.93 (d, J = 5.7 Hz, 2H), 3.54 (d, J = 5.8 Hz, 2H). ^{13}C NMR (100 MHz, DMSO-d_6, δ ppm): 180.57, 150.49, 149.67, 149.41, 145.68, 138.92, 135.79, 128.76, 128.04, 124.43, 123.39, 122.82, 120.34, 117.37, 101.54, 42.22, 41.90. ESI mass spectrum m/z: calcd for $C_{21}H_{19}N_5S$, 373.1; found, 374.3 $[M + H]^+$.

Synthesis of $[Ir_2(ppy)_4Cl_2]$ (5). The chloro-bridged dimer $[Ir_2(ppy)_4Cl_2]$ was synthesized according to the literature.[14] A mixture of 2-ethoxyethanol and water (3/1 v/v) was placed in a flask containing $IrCl_3·3H_2O$ (0.71 g, 2 mmol) and 2-phenylpyridine (0.68 g, 4.4 mmol). The mixture was heated under reflux for 24 h. After the

dx.doi.org/10.1021/ic501417s | Inorg. Chem. 2014, 53, 11498−11506

mixture was cooled to room temperature, the yellow solid precipitate was filtered to give the crude cyclometalated Ir(III) chloro-bridged dimer. Yield: 0.95 g (89%).

Synthesis of Complex 1. A mixture of the cyclometalated Ir(III) chloro-bridged dimer $[Ir_2(ppy)_4Cl_2]$ (206 mg, 0.192 mmol) and 1-(2-(1,10-phenanthrolin-5-ylamino)ethyl)-3-phenylthiourea (144 mg, 0.384 mmol) in 50 mL of CH_2Cl_2/MeOH (1/1 v/v) was refluxed under an inert atmosphere of argon in the dark for 24 h. The solution was then cooled to room temperature, and NH_4PF_6 (1.92 mmol) was added to the solution. The mixture was evaporated to dryness, and the solid was dissolved in CH_2Cl_2 and purified by column chromatography on silica gel. The desired product was eluted with CH_2Cl_2/MeOH (100/1 v/v) and subsequently recrystallized from CH_2Cl_2/*n*-hexane. Complex **1** was isolated as yellow crystals. Yield: 320 mg (82%). ^{1}H NMR (400 MHz, DMSO-d_6, δ ppm): 9.73 (s, 1H), 9.11−9.04 (m, 1H), 8.38 (dd, J = 7.1, 2.7 Hz, 1H), 8.25 (d, J = 8.3 Hz, 2H), 8.19−8.14 (m, 1H), 8.02 (dd, J = 8.6, 5.1 Hz, 1H), 7.94 (dd, J = 7.3, 4.8 Hz, 3H), 7.88 (t, J = 7.8 Hz, 2H), 7.75 (dd, J = 8.3, 3.8 Hz, 2H), 7.46 (t, J = 5.3 Hz, 3H), 7.37−7.25 (m, 4H), 7.16−7.09 (m, 1H), 7.03 (qd, J = 7.3, 1.1 Hz, 4H), 6.94 (qd, J = 7.5, 1.2 Hz, 2H), 6.28 (dd, J = 12.7, 6.8 Hz, 2H), 3.92 (d, J = 1.3 Hz, 2H), 3.62 (dd, J = 11.5, 6.0 Hz, 2H). ^{13}C NMR (150 MHz, DMSO-d_6, δ ppm): 180.53, 166.94, 166.86, 150.74, 150.24, 149.02, 148.78, 146.99, 145.12, 144.03, 143.95, 140.08, 138.61, 135.31, 133.36, 133.12, 131.29, 131.16, 130.13, 128.86, 126.86, 125.73, 125.05, 124.60, 124.38, 123.78, 123.51, 122.27, 119.89, 98.57, 42.75, 41.96. ESI mass spectrum m/z: calcd for $C_{43}H_{35}N_7SIrPF_6$, 1018.4; calcd for $[C_{43}H_{35}N_7SIr]^+$, 874.2; found, 874.3 $[\mathbf{1} - PF_6]^+$.

Synthesis of Complex 2. Complex **1** (81 mg, 0.08 mmol) and $Hg(ClO_4)_2{\cdot}3H_2O$ (36 mg, 0.08 mmol) were stirred in acetonitrile (20 mL) for 10 h at room temperature. The solid that formed was removed by filtration. The solution was concentrated by evaporation. The product was purified by silica gel column chromatography with CH_2Cl_2/MeOH (100/1 v/v). The eluent was concentrated, and the residue was subsequently recrystallized from CH_2Cl_2/*n*-hexane. Complex **2** was isolated as yellow crystals. Yield: 67 mg (85%). ^{1}H NMR (400 MHz, DMSO-d_6, δ ppm): 10.07 (s, 1H), 9.11 (d, J = 8.1 Hz, 1H), 8.93 (s, 1H), 8.80 (s, 1H), 8.29 (d, J = 5.9 Hz, 4H), 8.14 (ddd, J = 20.9, 7.9, 5.3 Hz, 2H), 7.97 (d, J = 7.8 Hz, 2H), 7.90 (t, J = 7.8 Hz, 2H), 7.43 (m, 7H), 7.14−6.94 (m, 6H), 6.28 (d, J = 7.5 Hz, 2H), 4.40 (s, 1H), 4.25 (s, 1H), 3.96 (s, 2H). ESI mass spectrum m/z: calcd for $C_{43}H_{33}N_7IrPF_6$, 985.2068; calcd for $[C_{43}H_{33}N_7Ir]^+$, 840.2427; found, 840.2405 $[\mathbf{1} - H_2S - PF_6]^+$.

UV−Vis Absorption and Phosphorescence Spectral Studies. UV−vis absorption spectra were recorded on a Jena SPECORD 50 PLUS UV/vis spectrophotometer. Phosphorescence spectra were measured using a Hitachi F-7000 spectrofluorophotometer equipped with a xenon lamp, 1.0 cm quartz cells, and 5.0/10.0 nm slits. For all measurements with **1**, the excitation wavelength was chosen as 380 nm and all spectra were recorded at 25 °C. The luminescence lifetime was determined on an Edinburgh FLS920 time-correlated pulsed single-photon-counting instrument. Luminescence quantum yields at room temperature were measured by the optically dilute method[15] with an aerated aqueous solution of $[Ru(bpy)_3]Cl_2$ (Φ_{em} = 0.028) as the standard solution[7a,11c,16] and by using the equation

$$\Phi_u = \Phi_s \frac{D_u A_s n_u^2}{D_s A_u n_s^2}$$

where Φ is the quantum yield, D is the integrated area of the emission spectrum, A is the absorbance at the excitation wavelength, n is the refractive index of the solution, and the subscripts u and s refer to the unknown and the standard, respectively.

Time-Resolved Luminescence Detection. Time-resolved emission spectra (TRES) were performed through a time-correlated single photon counting (TCSPC) technique by using a FLS920 instrument (Edinburgh, U.K.) with an LED laser (360 nm) as the excitation source. The luminescence signal from 450 to 780 nm was collected and recorded with a R928-P instrument at a step size of 5 nm. The TRES experiment was performed in duplicate using freshly prepared samples. In order to exhibit the emission peaks of the complex and Rhodamine 6G (as a typical fluorescent interference) simultaneously, different concentrations of **1** (50 μM) and Rhodamine 6G (1 μM) were used and mixed in acetonitrile (air-equilibrated) because of the stronger fluorescence of Rhodamine 6G. Delayed photoluminescence spectra acquired after 100 ns would eliminate most of the fluorescence from Rhodamine 6G. Thus, a photoluminescence spectrum at 100 ns delay was chosen and compared with the total photoluminescence spectrum.

Theoretical Calculations. Calculations were performed using the Gaussian 09 suite of programs.[17] The ground-state structures of the complexes were optimized using density functional theory (DFT) with Becke's three-parameter hybrid functional with the Lee−Yang−Parr correlation functional (B3LYP)[18] and 6-31+G(d)/LanL2DZ basis set. The LanL2DZ basis set was used to treat the iridium atom,[19] whereas the 6-31+G(d) basis set was used to treat all other atoms.[20] The excited-state-related calculations were carried out with time-dependent density functional theory (TD-DFT) with the optimized structure of the ground state (DFT 6-31+G(d)/LanL2DZ).[21] Fifteen singlet absorptions and three triplet emissions were obtained to determine the vertical excitation energies for **1** and **2** in acetonitrile using the time-dependent DFT (TD-DFT) calculations, respectively. The polarized continuum model method (CPCM) with acetonitrile as solvent was used to calculate all electronic structures in solution.[22] There are no imaginary frequencies in the frequency analysis of all calculated structures; therefore, each calculated structure expresses an energy minimum. To understand the nature of the excited state, the orbital analyses of the complexes were also performed. The contours of the HOMOs and LUMOs were plotted.

Cell Culture and Cytotoxicity Tests. SMMC-7721 cells were grown in RPMI-1640 medium supplemented with 10% heat-inactivated fetal calf serum and 1% penicillin/streptomycin. Cells (5×10^8 L^{-1}) were plated on 18 mm glass coverslips and allowed to adhere for 24 h at 37 °C under a humidified atmosphere containing 5% CO_2. Then cells were treated with **1** (10 μM) and incubated for 30 min. Subsequently, the cells were treated with 100 μM $Hg(ClO_4)_2{\cdot}3H_2O$ for another 30 min. The cells were rinsed with PBS three times to remove free compound and ions. SMMC-7721 cells only incubated with 10 μM **1** for 30 min acted as a control.

Standard 3-(4,5-dimethylthiazole)-2,5-diphenyltetraazolium bromide (MTT) assay procedures were used to test the cytotoxicity of complex **1**. SMMC-7721 cells were placed in 96-well microassay culture plates (1×10^4 cells per well) and grown for 24 h at 37 °C in a 5% CO_2 incubator. Complex **1** was then added to the wells to achieve final concentrations of 5, 10, 25, and 50 μM. Control wells were prepared by addition of culture medium (100 μL). The plates were incubated at 37 °C in a 5% CO_2 incubator for another 24 h. Upon completion of the incubation, stock MTT dye solution (20 μL, 5 mg/mL) was added to each well. After 4 h, dimethyl sulfoxide (150 μL) was added to solubilize the MTT formazan. An enzyme-linked immunosorbent assay (ELISA) reader (Bio-Rad, Model 550) was used to measure the OD570 (absorbance value) of each well referenced at 655 nm. Each experiment was repeated at least three times to obtain the mean values.

Confocal Luminescence Imaging. Confocal luminescence images of SMMC-7721 cells were carried out on an Olympus FV1000 laser scanning confocal microscope and a 100× oil-immersion objective lens. Emission was collected at 510−610 nm for the SMMC-7721 cells.

RESULTS AND DISCUSSION

Synthesis and Characterization. The synthetic route to chemodosimeter **1** is depicted in Scheme 1. First, the 1,10-phenanthroline ligand linked to a thiourea unit was synthesized through the nucleophilic substitution of 5-amino-1,10-phenanthroline with 2-bromoethylamine hydrobromide, which was subsequently reacted with phenyl isothiocyanate. The chloro-bridged dinuclear cyclometalated Ir(III) precursor $[Ir_2(ppy)_4Cl_2]$ was obtained according to a method described

dx.doi.org/10.1021/ic501417s | Inorg. Chem. 2014, 53, 11498−11506

in the literature. Then, substitution of the chlorides in $[Ir_2(ppy)_4Cl_2]$ with the thiourea-appended phenanthroline ligand was performed, followed by metathesis with NH_4PF_6 to afford chemodosimeter **1**. To make sure the mercury-induced intramolecular cyclic guanylation of the thiourea moiety occurred, **2** was isolated from the reaction of **1** with 1 equiv of $Hg(ClO_4)_2$ in acetonitrile at room temperature. The compounds were efficiently synthesized and fully characterized (see the Supporting Information).

Photophysical Properties. The absorption and emission spectra of chemodosimeter **1** and isolated product **2** in acetonitrile solutions are shown in Figure 1. The UV–vis

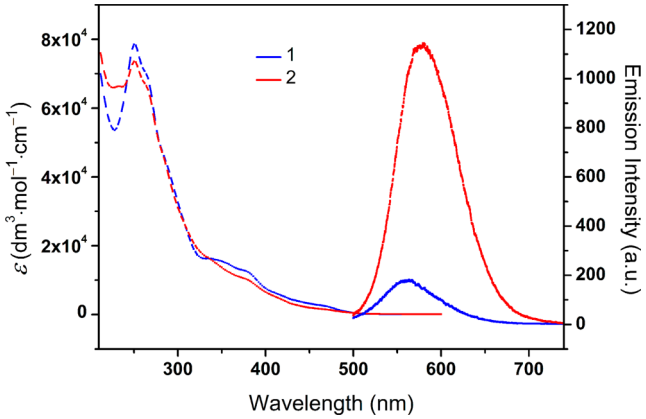

Figure 1. UV–vis absorption (dash lines) and emission (solid lines) spectra of **1** (blue) and **2** (red) in acetonitrile. Conditions: [**1**] = [**2**] = 10 μM, λ_{ex} 380 nm.

absorption spectra of the two complexes both displayed intense absorption bands with extinction coefficients on the order of $\sim 10^5$ dm^3 mol^{-1} cm^{-1} in the wavelength region shorter than 320 nm, which were assigned to the spin-allowed ligand-centered (^{1}LC) transitions. In addition, a moderately intense absorption band at about 320–480 nm with extinction coefficients (ε) of $\sim 10^4$ dm^3 mol^{-1} cm^{-1}, which could be assigned to an overlap of the spin-allowed metal-to-ligand charge-transfer transition (^{1}MLCT, dπ(Ir) → π^*(ppy and **L**)), ligand-to-ligand charge-transfer transition (^{1}LLCT, π(ppy) → π^*(**L**)) and intraligand charge-transfer transition (^{1}ILCT, π(**L**) → π^*(**L**) and π(ppy) → π^*(ppy)), as confirmed by TD-DFT calculations (Figures S1 and S2 and Tables S1–S4, Supporting Information).

In the phosphorescence spectrum, chemodosimeter **1** (10 μM) exhibited a weak and single emission band at ca. 560 nm at ambient temperature. The weak emission comes mainly from a ^{3}ILCT excited state, which was further confirmed by the TD-DFT calculations (Figure S3 and Tables S5 and S6, Supporting Information). In air-equilibrated acetonitrile, the quantum yield (Φ_{em}) of **1** was measured to be 0.003 and the average lifetimes[23] monitored at 560 nm were measured to be τ = 390 ns. In contrast, isolated product **2** displayed a stronger emission with quantum yields of 0.019 in air-equilibrated acetonitrile. The stronger emission was attributed to an admixture of ^{3}MLCT (dπ(Ir) → π^*(**L**)) and ^{3}LLCT (π(ppy) → π^*(**L**)), which was further confirmed by the TD-DFT calculations (Figure S4 and Tables S7 and S8, Supporting Information). In addition, the average lifetime monitored at 573 nm of **2** in air-equilibrated acetonitrile was also measured to be τ = 93 ns, which is suitable for time-resolved luminescent detection.

It is worth mentioning that chemodosimeter **1** exhibited a large Stokes shift (>180 nm), which is larger than that of a conventional fluorescence probe whose Stokes shift is only 20–30 nm. The large Stokes shift can be used for eliminating the interference from scattered light.

Selectivity and Cation-Competitive Experiments. The metal ion recognition capability of chemodosimeter **1** was systematically carried out for diverse metal ions in acetonitrile/HEPES buffer (10 mM, 4/6 v/v, pH 7.4) solutions. Variations of emission spectra of **1** (10 μM), recorded within 5 min after the addition of 10 equiv of these common metal ions, are displayed in Figure 2a. Only the addition of Hg^{2+} ion could

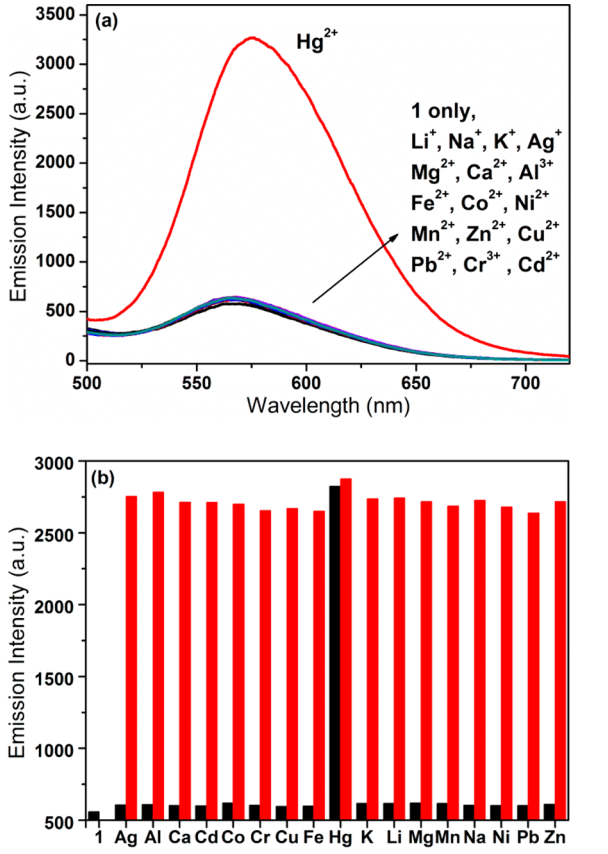

Figure 2. (a) Luminescence spectra of **1** (10 μM) upon the addition of various metal ions (Li^+, Na^+, K^+, Mg^{2+}, Ca^{2+}, Al^{3+}, Fe^{3+}, Co^{2+}, Ni^{2+}, Cu^{2+}, Cr^{3+}, Pb^{2+}, Cd^{2+}, Ag^+, Mn^{2+}, Zn^{2+}, and Hg^{2+}) within 5 min in acetonitrile/HEPES buffer (10 mM, 4 6 v/v, pH 7.4) solutions. (b) Relative luminescence intensities of **1** (10 μM) in acetonitrile/HEPES buffer (10 mM, 4/6 v/v, pH 7.4) solutions at 560 nm. Black bars represent addition of 10 equiv of various metal ions to the solution, and red bars represent addition of 10 equiv of Hg^{2+} and 10 equiv of various metal ions to the solution. Conditions: λ_{ex} 380 nm.

cause a prominent emission enhancement with slight red shift in their emission maxima, whereas very weak variations in the emission spectra of **1** were observed upon addition of other metal ions, such as Li^+, Na^+, K^+, Mg^{2+}, Ca^{2+}, Al^{3+}, Fe^{3+}, Co^{2+}, Ni^{2+}, Cu^{2+}, Cr^{3+}, Pb^{2+}, Cd^{2+}, Ag^+, Mn^{2+}, and Zn^{2+}. Therefore, chemodosimeter **1** displayed a turn-on phosphorescence response and high selectivity in sensing Hg^{2+} ion. Moreover, cation-competitive experiments were also carried out by adding Hg^{2+} ion to solutions of **1** in the presence of other metal ions. As shown in Figure 2b, whether in the absence or in the presence of the other metal ions, obvious spectral changes were

dx.doi.org/10.1021/ic501417s | Inorg. Chem. 2014, 53, 11498–11506

observed for **1** only upon addition of Hg^{2+} ion. The results indicate that the sensing of Hg^{2+} ion by **1** is hardly affected by these commonly coexistent ions.

Hg(II) Titration Experiments. Efforts were then made to understand the spectral changes of **1** and nature of the mercury-induced response. The emission spectral changes of **1** (10 μM) were measured with different concentrations of Hg^{2+} (0–20 μM) in acetonitrile/HEPES buffer (10 mM, 4/6 v/v, pH 7.4) solutions. As shown in Figure 3a, with continuous

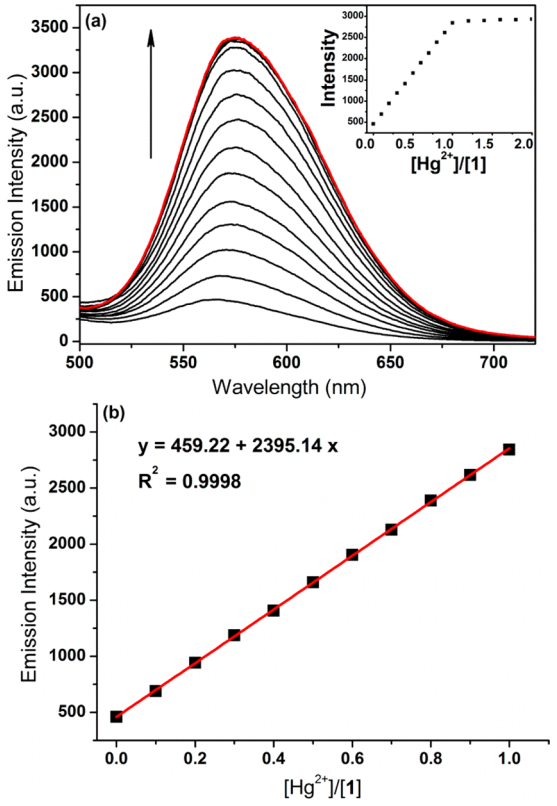

Figure 3. (a) Luminescence spectra of **1** (10 μM) upon titration with Hg^{2+} (0–20 μM) in acetonitrile/HEPES buffer (10 mM, 4/6 v/v, pH 7.4) solutions. Inset: titration curve of **1** with Hg^{2+}. (b) Luminescence linear changes of **1** (10 μM) upon titration with Hg^{2+} (0–10 μM) in acetonitrile/HEPES buffer (10 mM, 4/6 v/v, pH 7.4) solutions at 560 nm.

addition of Hg^{2+} into **1**, a weak emission band at 560 nm underwent a ca. 6-fold enhancement and the emission intensity increased linearly with the amount of Hg^{2+} in the range 0–10 μM (Figure 3a, insert), suggesting that the mercury-promoted cyclic guanylation of the chemodosimeter has a 1/1 stoichiometry and a new species is only produced during the titration. From the linear equation (Figure 3b), the detection limit for Hg^{2+} was calculated to be 6.6 ppb at a signal to noise ratio (S/N) of 3, which is much lower than that for many reported Hg^{2+} sensors based on cyclometalated Ir(III) complexes[11,12,24] and shows that **1** is a promising tool for the quantitative determination of Hg^{2+} concentration.

Response Time Experiments. For a chemodosimeter, the emission response time depends on the rate of the reaction between the dosimeter molecule and the target species. Thus, the reaction kinetics for the time-dependent dosimetric response was evaluated between **1** and Hg^{2+} to shorten the reaction time and improve the detection efficiency. As shown in Figure 4, the time needed for the emission intensity of **1** (10 μM) to gradually reach a stable state at 560 nm was obviously

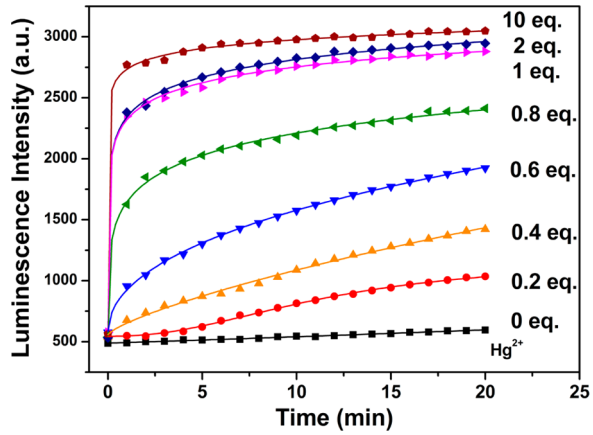

Figure 4. Time course of the luminescence response of **1** monitored at 560 nm over time with the addition of Hg^{2+} ions (0, 0.2, 0.4, 0.6, 0.8, 1.0, 2.0, 10 equiv) in acetonitrile/HEPES buffer (10 mM, 4/6 v/v, pH 7.4) solutions. Conditions: λ_{ex} 380 nm, λ_{em} 560 nm, [**1**] = 10 μM.

shortened with an increase in the ratio $[Hg^{2+}]/[\mathbf{1}]$ in acetonitrile/HEPES buffer (10 mM, 4/6 v/v, pH 7.4) solutions. When the concentration ratio $[Hg^{2+}]/[\mathbf{1}]$ was more than 1/1, the progress curve of the kinetic analysis clearly demonstrated that the emission intensity of **1** quickly increased in the first 2 min and reached a relative maximum within 5 min, suitable for rapid Hg^{2+} detection.

Effects of the pH. In addition, the effect of pH on the emission of **1** and the **1**–Hg^{2+} system was also investigated in acetonitrile/water (4/6 v/v) solutions (Figure 5). There was no

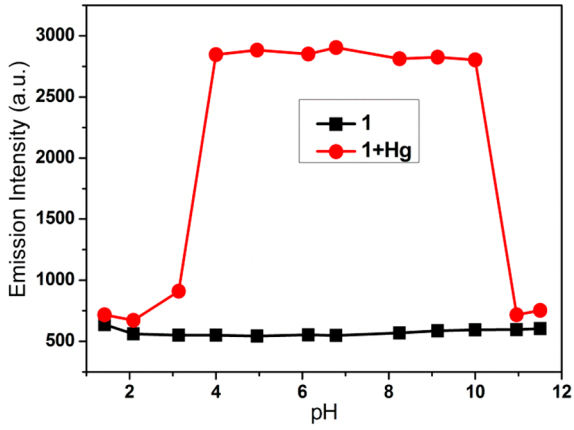

Figure 5. Luminescence intensity of **1** (10 μM) at 560 nm in the absence and presence of 10 equiv of Hg^{2+} as a function of pH in acetonitrile/water (4/6 v/v) solutions. Conditions: λ_{ex} 380 nm.

dramatic spectral change for chemodosimeter **1** at a variety of pH values, but it was still highly sensitive and stable for Hg^{2+} within the pH range 4–10, within which range most biological samples (5.25–8.93) can be tested. Chemodosimeter **1** failed to respond to Hg^{2+} ions at lower pH, which might be due to the protonation of the 1,10-phenanthroline group and the decomposition of the Ir(III) complex. However, the lack of response to Hg^{2+} at higher pH was mainly because the Hg^{2+} ion had been hydrolyzed. Considering the excellent sensing performances of chemodosimeter **1** in solution, it is possible

dx.doi.org/10.1021/ic501417s | Inorg. Chem. 2014, 53, 11498–11506

that **1** could be used in living cells without interference from pH effects.

Density Functional Theory (DFT) Calculations. To further understand the response mechanism and phosphorescence properties, time-dependent DFT (TD-DFT) calculations for **1** and cyclized product **2** were performed to estimate the corresponding transition energy. The ground-state geometries of the two complexes were first optimized, and the low-lying singlet−singlet transitions based on the optimized S_0 state geometry revealed that the excitations of **1** and **2** could be mainly assigned to an overlap of ^{1}LLCT/^{1}MLCT/^{1}ILCT, supported by UV−vis spectral profiles in the absorption around 320−480 nm, which implies that their different substituents give inappreciable changes in absorbance features for both complexes (Figures S1 and S2 and Table S1−S4, Supporting Information).

For calculated emission transitions, the distributions of the molecular orbitals and the calculated data are compared in Figure 6 and Table 1. In chemodosimeter **1**, the triplet

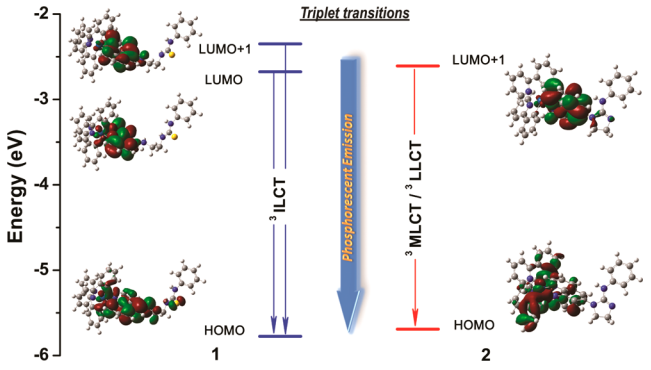

Figure 6. HOMO and LUMO distributions of complexes **1** and **2** corresponding to calculated triplet transitions.

excitations for **1** corresponding to the low-lying triplet−triplet transitions (557 nm) originate from HOMO → LUMO (36.5% contribution) and HOMO → LUMO+1 (63.5% contribution). As shown in Figure 6 and Table S5 (Supporting Information), the calculated HOMO of **1** is mainly localized on the phenanthroline ligand (61.92%) and thiourea group (26.10%), while the calculated LUMO and LUMO+1 of **1** are primarily localized on the phenanthroline ligand (91.42 and 91.59%, respectively). Hence, the inefficient phosphorescence emission of chemodosimeter **1** may be attributed to the ^{3}ILCT (π(**L**) → π^*(**L**)) state, dominated by the electron transfer from the thiourea group to phenanthroline in part. For cyclized product **2**, the triplet excitations corresponding to the low-lying triplet−triplet transitions (563 nm) mainly originate from the HOMO → LUMO+1 (96.4% contribution). The distribution of LUMO+1 is similar to that of LUMO+1 of **1** and is mainly localized on the phenanthroline ligand (93.99%). However, the distribution of the HOMO of **2** is significantly different from that of **1** and resides on the Ir(III) center (34.18%) and phenylpyridine ligands (47.84%) (Table S7, Supporting Information). Thus, an admixture of ^{3}MLCT (dπ(Ir) → π^*(**L**)) and ^{3}LLCT (π(ppy) → π^*(**L**)) is responsible for the triplet−triplet transitions of **2**, improving the phosphorescent efficiency of the Ir(III) complex. Therefore, the significant enhancement in emission intensity for **2** may arise from a less nonradiative process in the rigid molecular structure and the variation of transition characters.[25] Accordingly, a turn-on phosphorescent probe for sensing Hg^{2+} based on Ir(III) complex has been realized.

Mechanism of the Sensing of Hg(II). ESI mass spectral changes of **1** in the absence and presence of Hg^{2+} ion were employed to provide direct evidence. The chemodosimeter **1** displayed a characteristic peak of $[\mathbf{1} - PF_6]^+$ at m/z 874.3. However, after the addition of Hg^{2+} ion, the peak completely disappeared and a new peak arose at m/z 840.2405 assigned to $[\mathbf{1} - PF_6 - H_2S]^+$. By reacting **1** with 1 equiv of Hg^{2+} at room temperature, ^{1}H NMR spectra of the isolated product **2** were measured. Two peaks corresponding to N−H groups in the thiourea unit of **1** disappeared and another N−H group in the thiourea unit at δ 9.73 ppm shifted downfield (Figure S6, Supporting Information). In addition, the chemical shifts of two methylene groups were all shifted downfield and one of them was split, supporting the Hg^{2+}-triggered desulfurization reaction and cyclization of the chemodosimeter **1** to form a rigid structure. Thus, a mechanism for the reaction of **1** with Hg^{2+} is depicted in Scheme 2.

Scheme 2. Proposed Mechanism for the Hg^{2+}-Induced Intramolecular Cyclic Guanylation of the Thiourea Moiety

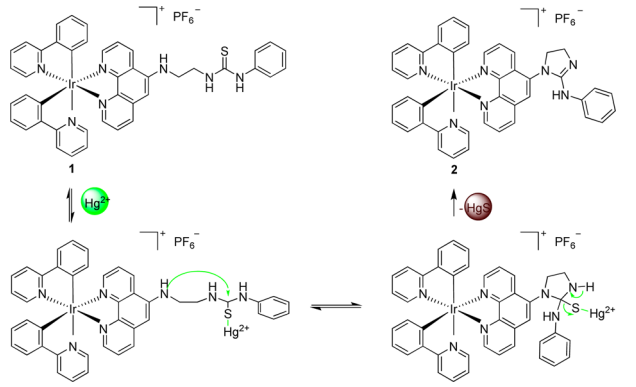

Application in Time-Resolved Luminescence Assays. In practical applications, the validity and accuracy of the chemsensors encounter inevitable interference with undesirable scattered light and/or shorter-lived background fluorescence. The most attractive merit of **1** is the long emission lifetime of its phosphorescent signal. For chemodosimeter **1**, the average lifetime monitored at 560 nm was τ = 390 ns, which is long enough to do TRES experiments. To demonstrate the advantage of **1**, the fluorescent dye Rhodamine 6G, with a short emission lifetime of 3.66 ns (1×10^{-4} mol L^{-1}) in

Table 1. TD-DFT Calculations for the Triplet Transition and MO Contributions of 1 and 2 in Acetonitrile

complex	state	transition	contribution/%	E/nm (eV)	assignment
1	T_1	HOMO → LUMO	36.5	557 (2.23)	^{3}ILCT
		HOMO → LUMO+1	63.5		^{3}ILCT
2	T_1	HOMO → LUMO+1	96.4	563 (2.20)	^{3}MLCT/^{3}LLCT

dx.doi.org/10.1021/ic501417s | Inorg. Chem. 2014, 53, 11498−11506

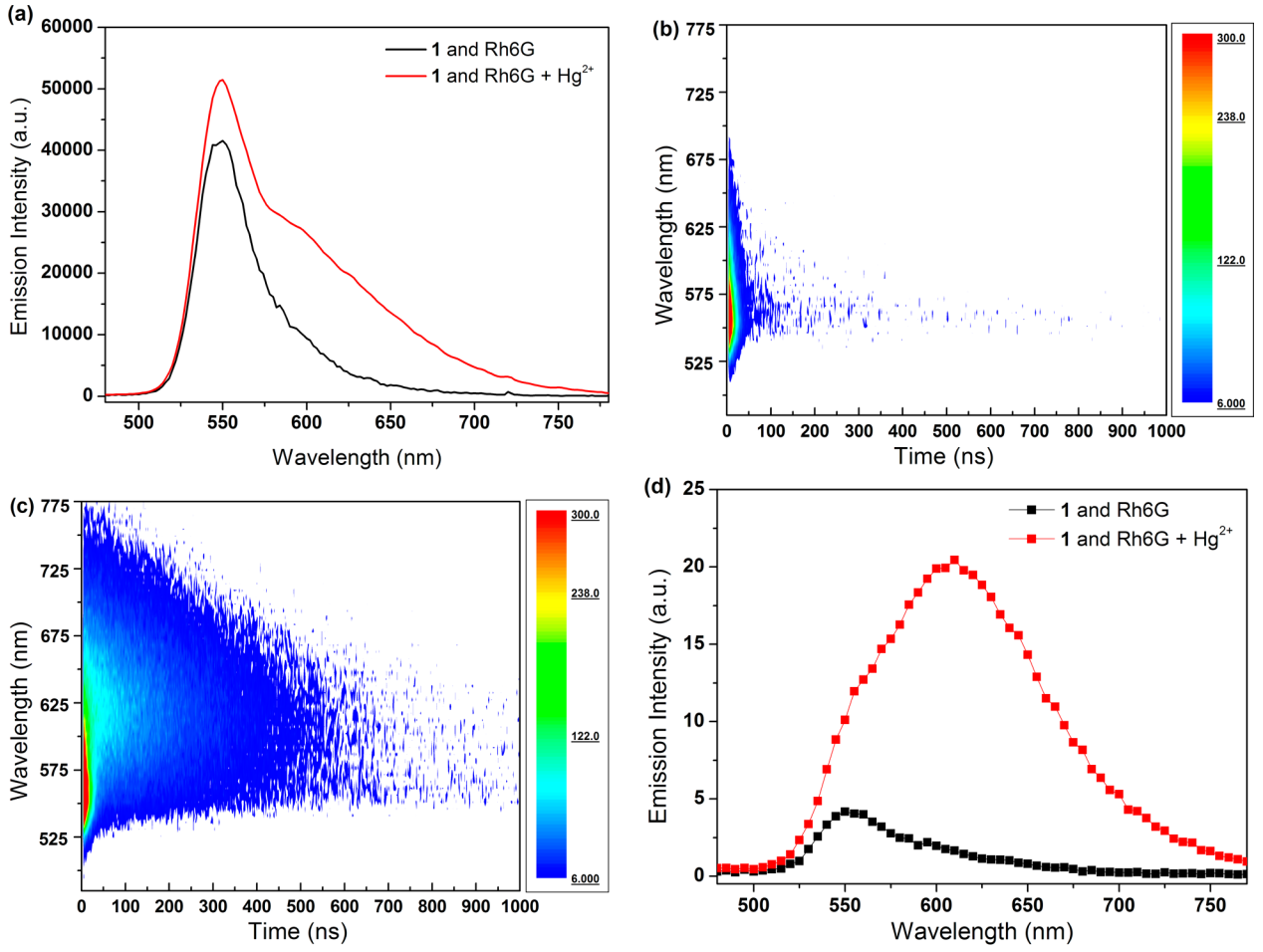

Figure 7. (a) Steady-state photoluminescence of chemodosimeter **1** containing Rhodamine 6G in the absence and presence of Hg^{2+}. (b, c) Time-resolved emission spectra of a mixture of chemodosimeter **1** and Rhodamine 6G before (b) and after (c) addition of Hg^{2+}. (d) Time-gated photoluminescence spectrum acquired after a 100 ns delay of chemodosimeter **1** containing Rhodamine 6G in the absence and presence of Hg^{2+}. Conditions: [**1**] = 50 μM, [Rh 6G] = 1 μM, [Hg^{2+}] = 250 μM.

acetonitrile,[26] was selected as a typical signal interference, whose emission can significantly overlap with the phosphorescence of **1** (Figure S7, Supporting Information). The steady-state photoluminescence spectra were recorded as shown in Figure 7a. As shown in Figure 7a, under 380 nm excitation, the obvious maximum emission at 550 nm was assigned to the strongly fluorescent Rhodamine 6G and the phosphorescence emission of probe **1**. When Hg^{2+} (5 equiv) was added, the fluorescence interference at 550 nm from Rhodamine 6G still existed and there was no obvious change in the steady-state emission spectra, which indicates the strong interference of background fluorescence to Hg^{2+} sensing. Then, the time-resolved emission spectra (TRES) of a mixture of **1** (50 μM) and Rhodamine 6G dye (1 μM) at room temperature were measured before and after addition of Hg^{2+} (Figure 7b,c). The time-gated photoluminescence spectrum acquired after a 100 ns delay of the mixture effectively removed most of the background fluorescence from Rhodamine 6G, though the emission at 550 nm belonging to Rhodamine 6G still remained, which might be due in part to energy transfer from Ir(III) complex **1** with a long-lifetime weak luminescence to the Rhodamine 6G. After addition of Hg^{2+}, the emission intensity was enhanced significantly in TRES, which realizes the time-resolved luminescence turn-on response to Hg^{2+} (Figure 7d). Although the technique suffers from low brightness because parts of the intensities will be lost by the time-gated removal, it is worth noting that these results exhibit the advantage of long-lifetime phosphorescence in eliminating the interference of background fluorescence and improving the signal-to-noise (S/N) ratio.

Application in Intracellular Hg(II) Imaging. The ability of **1** to detect Hg^{2+} within living SMMC-7721 cells was further tested by confocal luminescence imaging on the basis of the excellent sensing performance of **1** in aqueous solution. The human hepatoma cells (SMMC-7721) treated with 10 μM **1** alone for 30 min at 37 °C exhibited very weak emission (Figure 8a). Bright-field measurements after the treatment with **1** confirmed that the cells were viable throughout the imaging experiments. Overlays of confocal luminescence and bright-field images demonstrated that the luminescence was evident in the cytoplasm over the nucleus and membrane. When the **1**-treated cells were then exposed to 100 μM Hg^{2+} for 30 min at 37 °C, the whole cell displayed marked luminescence enhancement, which was clearly demonstrated by visual colors that match different luminescence intensities in the corresponding stained locations. Therefore, obvious luminescence changes indicated that **1** had good cell membrane permeability and can be applied to Hg^{2+} ion in the living cells, which is valuable for studying the uptake, bioaccumulation, and bioavailability of Hg^{2+} in living organisms. In addition, to demonstrate the bioimaging

dx.doi.org/10.1021/ic501417s | *Inorg. Chem.* 2014, 53, 11498−11506

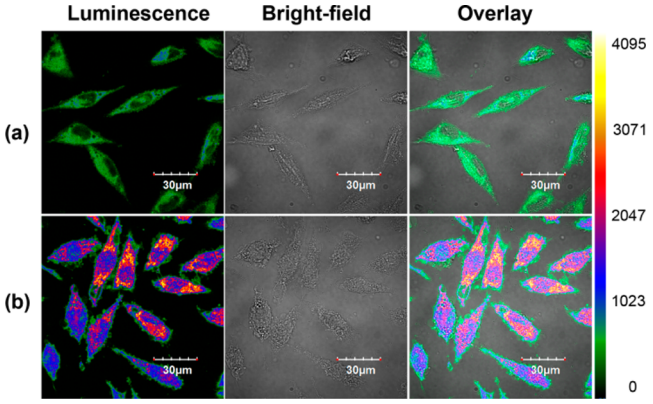

Figure 8. Confocal luminescence images of SMMC-7721 cells: (a) SMMC-7721 cells incubated with **1** (10 μM) for 30 min at 37 °C; (b) SMMC-7721 cells incubated with **1** for 30 min and then further incubated with 100 μM Hg^{2+} for 30 min at 37 °C. The color bar indicates intensity values.

usefulness, the cytotoxic activity of **1** against SMMC-7721 cells has been determined by using an MTT assay (Figure S8, Supporting Information). Although complex **1** at higher concentration (>25 μM) will kill the cell, the cell viability of the complex for SMMC-7721 cells remains above 80% upon incubation with **1** at the concentration (10 μM) of the cell imaging experiment for 24 h. When the concentration of **1** was 5 μM, the cell viability remained above 90%, which suggests that the chemodosimeter **1** has lower cytotoxicity at low concentration. The potential anticancer activity of complex **1** at high concentration will be investigated in the future.

CONCLUSION

In conclusion, we have rationally employed the "chemodosimeter approach" to develop a new phosphorescent probe based on a cyclometalated Ir(III) complex, which utilizes an irreversible Hg^{2+}-promoted desulfurization and cyclization reaction of the thiourea unit. The chemodosimeter exhibited a rapid turn-on phosphorescent response toward Hg^{2+} that was highly sensitive in aqueous media with a broad pH range of 4–10. Importantly, the utilization of the long emission lifetime and the time-resolved luminescent assay of chemodosimeter **1** for Hg^{2+} ions was developed successfully, which could eliminate effectively the interference from the short-lived fluorescence and improve distinctly the signal-to-noise ratio of the detection so that it is very helpful for the further design of excellent probes suitable for time-resolved photoluminescence techniques. Furthermore, the chemodosimeter **1** has been successfully used for bioimaging by using a confocal laser scanning microscope, which may be favorable for biological applications to monitor and research effectively Hg^{2+} in living cells.

ASSOCIATED CONTENT

Supporting Information

Figures and tables giving characterization data for the compounds, additional spectroscopic material, and TD-DFT calculations. This material is available free of charge via the Internet at http://pubs.acs.org.

AUTHOR INFORMATION

Corresponding Authors

*E-mail for X.-L. Tang: tangxiaol@lzu.edu.cn.
*E-mail for G.-L. Zhang: zhanggl@lzu.edu.cn.
*E-mail for W.-S. Liu: liuws@lzu.edu.cn.

Notes

The authors declare no competing financial interest.

ACKNOWLEDGMENTS

This work was supported by the NSFC (Grant 91122007, 21371083, 21001059, 21431002), the Fundamental Research Funds for the Central Universities (lzujbky-2014-192), and the Specialized Research Fund for the Doctoral Program of Higher Education (Grant No. 20110211130002).

REFERENCES

(1) (a) Harris, H. H.; Pickering, I. J.; George, G. N. *Science* **2003**, *301*, 1203. (b) Tchounwou, P. B.; Ayensu, W. K.; Ninashvili, N.; Sutton, D. *Environ. Toxicol.* **2003**, *18*, 149. (c) Stefansson, E. S.; Heyes, A.; Rowe, C. L. *Environ. Sci. Technol.* **2014**, *48*, 1957. (d) Tong, Y. D.; Zhang, W.; Chen, C.; Chen, L.; Wang, W. T.; Hu, X. D.; Wang, H. H.; Hu, D.; Ou, L. B.; Wang, X. J.; Wang, Q. G. *Environ. Pollut.* **2014**, *184*, 54.

(2) (a) Jana, A.; Kim, J. S.; Jung, H. S.; Bharadwaj, P. K. *Chem. Commun.* **2009**, 4417. (b) Lee, M. H.; Giap, T. V.; Kim, S. H.; Lee, Y. H.; Kang, C.; Kim, J. S. *Chem. Commun.* **2010**, 1407. (c) Duong, T. Q.; Kim, J. S. *Chem. Rev.* **2010**, *110*, 6280. (d) Chen, X.; Pradhan, T.; Wang, F.; Kim, J. S.; Yoon, J. *Chem. Rev.* **2012**, *112*, 1910. (e) Zhou, J.; Liu, Z.; Li, F. *Chem. Soc. Rev.* **2012**, *41*, 1323. (f) Yang, Y.; Zhao, Q.; Feng, W.; Li, F. *Chem. Rev.* **2013**, *113*, 192. (g) Carter, K. P.; Young, A. M.; Palmer, A. E. *Chem. Rev.* **2014**, *114*, 4564.

(3) (a) Cui, G. F.; Ye, Z. Q.; Zhang, R.; Wang, G. L.; Yuan, J. L. *J. Fluoresc.* **2012**, *22*, 261. (b) McMahon, B. K.; Gunnlaugsson, T. *Tetrahedron Lett.* **2010**, *51*, 5406. (c) Tan, H. L.; Zhang, Y. Q.; Chen, Y. *Sens. Actuators, B* **2011**, *156*, 120. (d) Tan, H.; Chen, Y. *J. Biomed. Opt.* **2012**, *17*, 017001.

(4) (a) You, Y.; Lee, S.; Kim, T.; Ohkubo, K.; Chae, W. S.; Fukuzumi, S.; Jhon, G. J.; Nam, W.; Lippard, S. J. *J. Am. Chem. Soc.* **2011**, *133*, 18328. (b) Liu, S. J.; Sun, H. B.; Ma, Y.; Ye, S. H.; Liu, X. M.; Zhou, X. H.; Mou, X.; Wang, L. H.; Zhao, Q.; Huang, W. *J. Mater. Chem.* **2012**, *22*, 22167. (c) Ma, Y.; Liu, S. J.; Yang, H. R.; Wu, Y. Q.; Sun, H. B.; Wang, J. X.; Zhao, Q.; Li, F. Y.; Huang, W. *J. Mater. Chem, B* **2013**, *1*, 319. (d) Shi, H. F.; Sun, H. B.; Yang, H. R.; Liu, S. J.; Jenkins, G.; Feng, W.; Li, F. Y.; Zhao, Q.; Liu, B.; Huang, W. *Adv. Funct. Mater.* **2013**, *23*, 3268. (e) Tang, Y.; Yang, H. R.; Sun, H. B.; Liu, S. J.; Wang, J. X.; Zhao, Q.; Liu, X. M.; Xu, W. J.; Li, S. B.; Huang, W. *Chem. Eur. J.* **2013**, *19*, 1311.

(5) (a) Zhao, Q.; Li, F.; Huang, C. *Chem. Soc. Rev.* **2010**, *39*, 3007. (b) You, Y.; Han, Y.; Lee, Y. M.; Park, S. Y.; Nam, W.; Lippard, S. J. *J. Am. Chem. Soc.* **2011**, *133*, 11488. (c) You, Y.; Nam, W. *Chem. Soc. Rev.* **2012**, *41*, 7061. (d) You, Y. *Curr. Opin. Chem. Biol.* **2013**, *17*, 699.

(6) (a) Zhao, Q.; Li, F.; Liu, S.; Yu, M.; Liu, Z.; Yi, T.; Huang, C. *Inorg. Chem.* **2008**, *47*, 9256. (b) Xu, W. J.; Liu, S. J.; Zhao, X. Y.; Sun, S.; Cheng, S.; Ma, T. C.; Sun, H. B.; Zhao, Q.; Huang, W. *Chem. Eur. J.* **2010**, *16*, 7125. (c) Reddy, G. U.; Das, P.; Saha, S.; Baidya, M.; Ghosh, S. K.; Das, A. *Chem. Commun.* **2013**, *49*, 255. (d) Fillaut, J. L.; Akdas-Kilig, H.; Dean, E.; Latouche, C.; Boucekkine, A. *Inorg. Chem.* **2013**, *52*, 4890.

(7) (a) Lee, P. K.; Law, W. H.; Liu, H. W.; Lo, K. K. *Inorg. Chem.* **2011**, *50*, 8570. (b) Han, Y.; You, Y.; Lee, Y. M.; Nam, W. *Adv. Mater.* **2012**, *24*, 2748. (c) Woo, H.; Cho, S.; Han, Y.; Chae, W. S.; Ahn, D. R.; You, Y.; Nam, W. *J. Am. Chem. Soc.* **2013**, *135*, 4771.

(8) (a) Chen, H.; Zhao, Q.; Wu, Y.; Li, F.; Yang, H.; Yi, T.; Huang, C. *Inorg. Chem.* **2007**, *46*, 11075. (b) Xiong, L.; Zhao, Q.; Chen, H.; Wu, Y.; Dong, Z.; Zhou, Z.; Li, F. *Inorg. Chem.* **2010**, *49*, 6402.

(9) Zhang, K. Y.; Li, S. P.; Zhu, N.; Or, I. W.; Cheung, M. S.; Lam, Y. W.; Lo, K. K. *Inorg. Chem.* **2010**, *49*, 2530.

(10) Li, Y.; Yoon, C. U.; Hyun, M. H. *Bull. Korean Chem. Soc.* **2011**, *32*, 122.

(11) (a) Zhao, Q.; Cao, T.; Li, F.; Li, X.; Jing, H.; Yi, T.; Huang, C. *Organometallics* **2007**, *26*, 2077. (b) Zhao, Q.; Liu, S.; Li, F.; Yi, T.;

Huang, C. *Dalton Trans.* **2008**, 3836. (c) Liu, Y.; Li, M.; Zhao, Q.; Wu, H.; Huang, K.; Li, F. *Inorg. Chem.* **2011**, *50*, 5969. (d) Wu, Y.; Jing, H.; Dong, Z.; Zhao, Q.; Wu, H.; Li, F. *Inorg. Chem.* **2011**, *50*, 7412. (e) Mei, Q.; Guo, Y.; Tong, B.; Weng, J.; Zhang, B.; Huang, W. *Analyst* **2012**, *137*, 5398. (f) Shi, H.; Liu, S.; An, Z.; Yang, H.; Geng, J.; Zhao, Q.; Liu, B.; Huang, W. *Macromol. Biosci.* **2013**, *13*, 1339.

(12) Lu, F.; Yamamura, M.; Nabeshima, T. *Dalton Trans.* **2013**, *42*, 12093.

(13) (a) Liu, B.; Tian, H. *Chem. Commun.* **2005**, 3156. (b) Wu, J.; Hwang, I.; Kim, K. S.; Kim, J. S. *Org. Lett.* **2007**, *9*, 907. (c) Lee, M. H.; Cho, B.; Yoon, J.; Kim, J. S. *Org. Lett.* **2007**, *9*, 4515. (d) Leng, B.; Zou, L.; Jiang, J.; Tian, H. *Sens. Actuators, B* **2009**, *140*, 162. (e) Lee, M. H.; Lee, S. W.; Kim, S. H.; Kang, C.; Kim, J. S. *Org. Lett.* **2009**, *11*, 2101.

(14) Sprouse, S.; King, K. A.; Spellane, P. J.; Watts, R. J. *J. Am. Chem. Soc.* **1984**, *106*, 6647.

(15) Demas, J. N.; Crosby, G. A. *J. Phys. Chem.* **1971**, *75*, 991.

(16) Nakamura, K. *Bull. Chem. Soc. Jpn.* **1982**, *55*, 2697.

(17) Frisch, M. J.; Trucks, G. W.; Schlegel, H. B.; Scuseria, G. E.; Robb, M. A.; Cheeseman, J. R.; Scalmani, G.; Barone, V.; Mennucci, B.; Petersson, G. A.; Nakatsuji, H.; Caricato, M.; Li, X.; Hratchian, H. P.; Izmaylov, A. F.; Bloino, J.; Zheng, G.; Sonnenberg, J. L.; Hada, M.; Ehara, M.; Toyota, K.; Fukuda, R.; Hasegawa, J.; Ishida, M.; Nakajima, T.; Honda, Y.; Kitao, O.; Nakai, H.; Vreven, T.; Montgomery, J. A., Jr.; Peralta, J. E.; Ogliaro, F.; Bearpark, M.; Heyd, J. J.; Brothers, E.; Kudin, K. N.; Staroverov, V. N.; Kobayashi, R.; Normand, J.; Raghavachari, K.; Rendell, A.; Burant, J. C.; Iyengar, S. S.; Tomasi, J.; Cossi, M.; Rega, N.; Millam, N. J.; Klene, M.; Knox, J. E.; Cross, J. B.; Bakken, V.; Adamo, C.; Jaramillo, J.; Gomperts, R.; Stratmann, R. E.; Yazyev, O.; Austin, A. J.; Cammi, R.; Pomelli, C.; Ochterski, J. W.; Martin, R. L.; Morokuma, K.; Zakrzewski, V. G.; Voth, G. A.; Salvador, P.; Dannenberg, J. J.; Dapprich, S.; Daniels, A. D.; Farkas, O.; Foresman, J. B.; Ortiz, J. V.; Cioslowski, J.; Fox, D. J. *Gaussian 09, Revision A.01*; Gaussian, Inc., Wallingford, CT, 2009.

(18) (a) Lee, C.; Yang, W.; Parr, R. G. *Phys. Rev. B* **1988**, *37*, 785. (b) Stephens, P. J.; Devlin, F. J.; Chabalowski, C. F.; Frisch, M. J. *J. Phys. Chem.* **1994**, *98*, 11623.

(19) Hay, P. J.; Wadt, W. R. *J. Chem. Phys.* **1985**, *82*, 270.

(20) (a) Hehre, W. J.; Ditchfield, R.; Pople, J. A. *J. Chem. Phys.* **1972**, *56*, 2257. (b) Hariharan, P. C.; Pople, J. A. *Theor. Chim. Acta* **1973**, *28*, 213. (c) Francl, M. M.; Pietro, W. J.; Hehre, W. J.; Binkley, J. S.; Gordon, M. S.; DeFrees, D. J.; Pople, J. A. *J. Chem. Phys.* **1982**, *77*, 3654.

(21) (a) Casida, M. E.; Jamorski, C.; Casida, K. C.; Salahub, D. R. *J. Chem. Phys.* **1998**, *108*, 4439. (b) Stratmann, R. E.; Scuseria, G. E.; Frisch, M. J. *J. Chem. Phys.* **1998**, *109*, 8218.

(22) (a) Barone, V.; Cossi, M. *J. Chem. Phys. A* **1998**, *102*, 1995. (b) Cossi, M.; Barone, V. *J. Chem. Phys.* **2001**, *115*, 4708. (c) Cossi, M.; Regar, N.; Scalmani, G.; Barone, V. *J. Comput. Chem.* **2003**, *24*, 669.

(23) Turro, N. J. *Modern Molecular Photochemistry*; Benjamin Cummings: Menlo Park, CA, 1978.

(24) Zeng, H.; Yu, F.; Dai, J.; Sun, H.; Lu, Z.; Li, M.; Jiang, Q.; Huang, Y. *Dalton Trans.* **2012**, *41*, 4878.

(25) (a) Zhao, N.; Wu, Y.; Wen, H.; Zhang, X.; Chen, Z. *Organometallics* **2009**, *28*, 5603. (b) Brandel, J.; Sairenji, M.; Ichikawa, K.; Nabeshima, T. *Chem. Commun.* **2010**, *46*, 3958. (c) Zhao, N.; Wu, Y.; Shi, L.; Lin, Q.; Chen, Z. *Dalton Trans.* **2010**, *39*, 8288.

(26) Guo, C.; Zhang, X. *Acta Opt. Sin.* **1983**, *3*, 64.